Liquid Crystals
Publication details, including instructions for authors and subscription information:
http://www.informaworld.com/smpp/title~content=t713926090

A dielectric study on the relaxation and switching behaviour of liquid crystals confined within a colloidal network

M. C. W. van Boxtel[a]; M. Wübbenhorst[b]; J. van Turnhout[b]; C. W. M. Bastiaansen[ac]; D. J. Broer[ad]
[a] Department of Polymer Technology, Eindhoven University of Technology, PO Box 513, 5600 MB Eindhoven, The Netherlands, [b] Department of Polymer Materials and Engineering, Delft University of Technology, Julianalaan 136, 2628 BL Delft, The Netherlands, [c] Dutch Polymer Institute, PO Box 902, 5600 AX Eindhoven, The Netherlands, [d] Philips Research Laboratories, Prof. Holstlaan 4, 5656 AA Eindhoven, The Netherlands,

Online publication date: 11 November 2010

To cite this Article van Boxtel, M. C. W. , Wübbenhorst, M. , van Turnhout, J. , Bastiaansen, C. W. M. and Broer, D. J.(2003) 'A dielectric study on the relaxation and switching behaviour of liquid crystals confined within a colloidal network', Liquid Crystals, 30: 2, 235 — 249
To link to this Article: DOI: 10.1080/0267829021000061132
URL: http://dx.doi.org/10.1080/0267829021000061132

LIQUID CRYSTALS, 2003, VOL. 30, NO. 2, 235–249

A dielectric study on the relaxation and switching behaviour of liquid crystals confined within a colloidal network

M. C. W. VAN BOXTEL†*, M. WÜBBENHORST‡, J. VAN TURNHOUT‡,
C. W. M. BASTIAANSEN†§ and D. J. BROER†¶

†Department of Polymer Technology, Eindhoven University of Technology,
PO Box 513, 5600 MB Eindhoven, The Netherlands
‡Department of Polymer Materials and Engineering,
Delft University of Technology, Julianalaan 136, 2628 BL Delft, The Netherlands
§Dutch Polymer Institute, PO Box 902, 5600 AX Eindhoven, The Netherlands
¶Philips Research Laboratories, Prof. Holstlaan 4, 5656 AA Eindhoven,
The Netherlands

(*Received 2 May 2002; accepted 19 September 2002*)

The molecular ordering and dynamics of a liquid crystal (LC E7) in the presence of a three-dimensional network of submicron particles have been studied by dielectric relaxation spectroscopy. The field-dependent orientation of the LC was quantified by the director order parameter and modelled by use of a three-phase model. The influence of the colloidal network on the molecular dynamics was assessed from the dielectric spectra, e.g. from the position of relaxation peaks as well as from the strength of the two principal relaxations (α and λ). The spectra changed noticeably upon application of an increasing d.c. bias. A reduction of the threshold field was observed upon addition of colloidal particles to the LC. This was associated with a switching between two metastable states induced by anchoring on the filler particles. Modelled spectra were found to be in good agreement with the experimental data. The modelling showed that the confined LC phase is composed of two fractions, viz. an ordered and a disordered one with different molecular mobilities. Furthermore, switching experiments were conducted at various temperatures in order to evaluate the impact of the colloidal network on the (temperature-dependent) orientational behaviour of the LC molecules. For the colloid-filled LC higher conductivities were found, which gave rise to longer switch-off times.

1. Introduction

The effect of confinement of liquid crystals on their physical properties, such as orientational order and phase transitions, has been addressed in several studies [1]. These studies were usually concerned with liquid crystals in random porous media like silica aerosils [2] or glassy materials [3–5], in polymer matrices (polymer dispersed liquid crystals, PDLCs) [6, 7], in anisotropic gels [8] or in silica-filled nematics [9–11]. In most cases, the molecular ordering and phase behaviour of the liquid crystal (LC) were probed by differential scanning calorimetry (DSC) [2, 9] or nuclear magnetic resonance (NMR) [7, 12]. Due to the high surface to volume ratio, the physical behaviour of confined LCs was found to be altered strongly compared with that of the bulk LC. The changes depend on the size and size distribution of the confining cavities. In recent years, dielectric relaxation spectroscopy (DRS) has been employed as a tool to analyse the behaviour of LCs in restricted geometries [5, 6, 11, 13]. Apart from revealing the modification of phase transitions and spatial inhomogeneities in the director order, this method also provides information about the impact of surface interactions on the dynamics of the LC molecules.

Here, we are concerned with another type of material that can be classified as a confined system, namely a colloidal dispersion in a nematic LC. Particle dispersions in an anisotropic medium show features that are very distinct from those of their isotropic analogues. The peculiar behaviour of particles immersed in an LC, regarding the introduction of topological defect phenomena, has been the subject of a number of studies in recent years and is nowadays understood quite well [14–17].

*Author for correspondence; e-mail: marysia@wish.nl

Liquid Crystals ISSN 0267-8292 print/ISSN 1366-5855 online © 2003 Taylor & Francis Ltd
http://www.tandf.co.uk/journals
DOI: 10.1080/0267829021000061132

A few years ago the first evidence was found for the segregation of a lyotropic LC, filled with small 120 nm size latex particles, into a particle-rich isotropic phase and a particle-poor nematic phase, upon passing through the isotropic–nematic phase transition [18]. In recent years, more detailed reports have appeared on this typical collective aggregation behaviour and on the resulting interesting properties of colloidal dispersions in an LC [19–23]. For instance, a surprising quasi-solid behaviour was detected at zero flow for such two-phase materials. This significantly facilitates the handling and processing of these so-called soft-solid materials with respect to a pure LC. In previous studies, we have investigated these new materials for application in both twisted nematic (TN) type and light scattering type electro-optical switches [19, 24]. Electro-optical switching experiments indicated that, in spite of the solid-like behaviour of the LC-colloidal dispersions on a macroscopic scale, the rotational mobility of the LC on a molecular scale is still maintained, albeit modified by the presence of the confining colloidal network. In view of this, we have suggested the production of displays based on LC-colloidal dispersions via continuous processing methodologies [19].

To our knowledge, anisotropic colloidal dispersions have not yet been analysed using dielectric relaxation spectroscopy. Therefore, DRS experiments were conducted in order to assess the impact of the colloidal network on the relaxation behaviour, the spatial inhomogeneities in the director order of the LC, and the switching dynamics of the LC molecules.

2. Experimental

2.1. *Materials and sample preparation*

The liquid crystal material was LC E7 ($n_e = 1.7462$, $n_o = 1.5216$) [25], a four-component liquid crystal mixture of cyanobiphenyls and a cyanoterphenyl purchased from Merck Ltd (Poole, England), containing 51% 4-*n*-pentyl-4′-cyanobiphenyl (5CB), 25% 4-*n*-heptyl-4′-cyanobiphenyl (7CB), 16% 4-*n*-octyloxy-4′-cyanobiphenyl (80CB) and 8% 4-*n*-pentyl-4″-cyano-*p*-terphenyl (5CT) [26]. According to the manufacturer, the density of the LC E7 is approximately equal to 1.0 g ml^{-1}.

Highly crosslinked, 630 nm size polymeric filler particles were prepared via dispersion polymerization of methyl methacrylate (~75 wt %) and a technical grade divinylbenzene (DVB55, ~25 wt %) in *n*-heptane, as described elsewhere [24]. Liquid crystalline colloidal dispersions were made by adding a pre-set amount of LC E7 to a pre-set amount of the dried colloids. Then chloroform was added and the colloidal particles homogeneously dispersed by ultrasonic mixing. The chloroform was evaporated from the mixture by drying for 24 h in a vacuum chamber at room temperature. Subsequently, the dried material was heated to 120–150°C, which is well above the nematic–isotropic phase transition of E7 at ~60°C. After slow cooling to room temperature, opaque soft solid-like LC-colloidal dispersions were obtained.

Electro-optical cells were filled with the preheated LC-colloidal dispersions in the isotropic state by capillary action at 150°C. After filling, the cells were cooled to room temperature. As soon as the isotropic–nematic transition temperature was passed, the cell appearance turned from transparent to opaque, depending on the material composition.

2.2. *Confocal laser scanning microscopy (CLSM)*

The morphology of the LC-colloidal dispersions confined in twisted nematic (TN) electro-optical cells with a cell gap of 7 μm was studied in three dimensions by use of a Zeiss laser scanning microscope (LSM 510). This apparatus employs a pinhole to eliminate light from regions outside the focal plane. By moving the focal plane along the *z*-direction within the sample by pre-set steps of 0.1 μm, a three-dimensional stack is built up from the single optical slices. The microscope was operated in the reflection mode, whereby the refractive index difference between the colloidal and the LC phase produced the optical contrast. Monochromatic laser light with a wavelength of 540 nm was used for illumination of the sample cells. The laser light was focused with a plan-apochromat 63 × /1.4 oil-immersion objective lens.

2.3. *Dielectric relaxation spectroscopy (DRS)*

The dielectric properties of the LC-colloidal dispersions were studied by means of a broadband dielectric spectrometer covering a frequency range from 10^{-2} to 10^6 Hz. This spectrometer utilizes a combination of two measurement systems with overlapping frequency ranges: (1) a frequency response analyser (Schlumberger 1260) equipped with a dielectric interface (developed by TNO) for frequencies between 10^{-2} and 10^4 Hz, and (2) a Hewlett-Packard 4284A precision LCR-meter for frequencies between 10^2 and 10^6 Hz. The sample was placed in a nitrogen cryostat (Novocontrol), whose temperature was controlled to a stability better than ±0.05 K.

Dielectric experiments were performed on 17.8 μm parallel electro-optical cells filled with colloidal dispersions with varying colloid content. For reference purposes, a 5.0 μm electro-optical cell filled with pure E7 was also used. These glass cells were inserted between gold-plated circular brass electrodes of the dielectric cell. In order to provide electrical contact between the inner

conducting indium tin oxide (ITO) layers of the electro-optical cells and the (outer) sample electrodes, conductive paths around the edges were made by means of silver paint.

The linear dielectric response of the samples was probed with a low a.c. voltage, usually 0.3 V for 17.8 μm cells, in order to prevent changes in the director order due to the probing field. When we were interested in the electric field-induced homeotropic alignment, the small a.c. voltage was superimposed by a d.c. bias of up to 40 V. All dielectric spectra were corrected for the (contact) resistance of the electrodes using an equivalent circuit model.

3. Results and discussion

3.1. *Morphology*

Figure 1 shows a typical three-dimensional CSLM image obtained for a 6.4 wt % 630 nm colloid E7 mixture in a 7 μm thick TN cell. The middle area of the orthogonal image represents just one optical slice of a three-dimensional stack of collected images in the xy-plane. The two side views show the morphology development in the *z*-direction, where the intersecting lines in the xy-plane slice the sample. The light intensity of the collected images gradually decreases with increasing penetration depth, as the light loss due to multiple scattering phenomena becomes more significant with increasing path length of the laser light.

From the confocal micrograph it is clearly visible that the colloids have assembled into larger aggregates that are partly interconnected forming a three-dimensional network. According to our previous study this peculiar spinodal morphology arises from the exclusion of colloids from emerging nematic domains during quenching of the (isotropic) dispersion below the isotropic–nematic transition of the LC [19]. The network structure seems to vary only slightly in the third dimension. It should be noted that in LC dispersions with another colloidal fraction, in particular those with 2.7 wt % colloids, a similar network structure was found. The size of the LC-rich regions confined within the colloidal network clearly increased for lower colloid fractions.

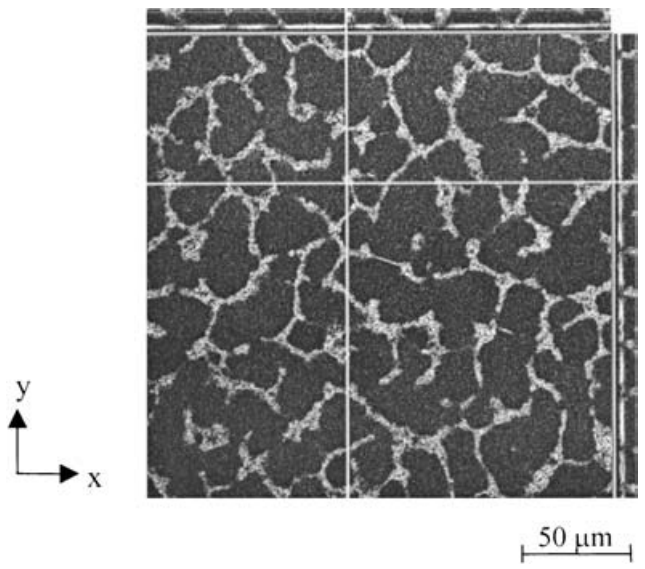

Figure 1. Confocal orthogonal microscopic image of a colloid/E7 mixture containing 6.4 wt % 630 nm poly(methyl methacrylate-*co*-divinylbenzene) colloidal particles, confined within a 7 μm TN electro-optical cell. The particles are seen to aggregate in a network. Two side views are shown on the top and on the right of the main image.

3.2. *Dielectric measurements*

3.2.1. *Determination of the director order parameter S_d*

Since dielectric spectroscopy enables the determination of the director order parameter S_d from the dielectric spectra, this method is particularly suitable for quantifying the impact of the colloidal network on the orientational behaviour of the LC and LC-colloidal dispersions. Three schematic spectra of the permittivity $\varepsilon'(f)$ are displayed in figure 2; for the homeotropic state $\varepsilon'_{\parallel}$, the planarly aligned state $\varepsilon'_{\perp}$ and the isotropic state $\varepsilon'_{iso} = (\varepsilon'_{\parallel} + 2\varepsilon'_{\perp})/3$[27].

According to Attard *et al.* [28], the three components of the complex dielectric constant $\varepsilon^* = \varepsilon' - i\varepsilon''$ of a uniaxial liquid crystal, which is assumed to be built up of many domains, can be linked to the director order

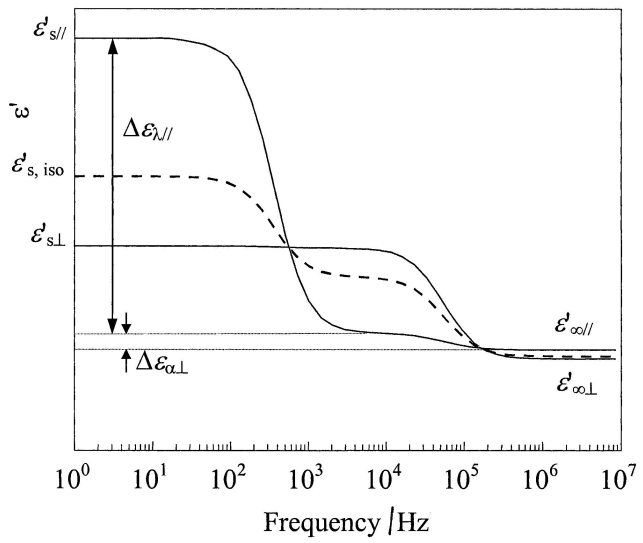

Figure 2. Dielectric spectra of $\varepsilon'(f)$ for a liquid crystal in the planar (⊥), homeotropic (∥), and isotropic state (schematic). They show two relaxation processes, the one at low frequencies is called λ, the one at high frequencies α.

parameter S_d by:

$$\varepsilon_z^* = \varepsilon_\parallel^*(1+2S_d)/3 + 2\varepsilon_\perp^*(1-S_d)/3 = (\varepsilon_\parallel^* + 2\varepsilon_\perp^*)/3 + 2(\varepsilon_\parallel^* - \varepsilon_\perp^*)S_d/3 \quad (1)$$

and

$$\varepsilon_x^* = \varepsilon_y^* = \varepsilon_\parallel^*(1-S_d)/3 + \varepsilon_\perp^*(2+S_d)/3 = (\varepsilon_\parallel^* 2\varepsilon_\perp^*)/3 - (\varepsilon_\parallel^* - \varepsilon_\perp^*)S_d/3 \quad (2)$$

where $\varepsilon_\parallel^*$ and $\varepsilon_\perp^*$ are the complex permittivities in the fully homeotropically and planarly aligned state, respectively, while ε_x^*, ε_y^* and ε_z^* denote the complex permittivities measured in the x-, y- and z-directions of the electric field. In the isotropic state, we have $S_d = 0$, so that $\varepsilon_{x,y,z,\mathrm{iso}}^* = (\varepsilon_\parallel^* + 2\varepsilon_\perp^*)/3$. For a parallel plate capacitor, in which the electric field is directed along the z-axis, we can invoke equation (1) for calculating S_d. Taking the real part of the dielectric constant ε_z' we obtain:

$$S_d = \frac{3\varepsilon_z' - (\varepsilon_\parallel' + 2\varepsilon_\perp')}{2(\varepsilon_\parallel' - \varepsilon_\perp')} = \frac{3(\varepsilon_z' - \varepsilon_{z,\mathrm{iso}}')}{2(\varepsilon_\parallel' - \varepsilon_\perp')}. \quad (3)$$

The imaginary part of the dielectric constant ε_z'' yields a similar equation. We have measured the dielectric spectra of pure E7 as well as of the colloidal mixtures with 2.7 and 6.4 wt % filler particles at -40°C. At this temperature the conduction losses are low, and so the two principal relaxation processes (α, λ) could be measured conveniently in the frequency range accessible. The results are plotted in figures 3(*a*) and 3(*b*) which show the dielectric spectra in the non-addressed (p-aligned) state as well as in the addressed (h-aligned) state. If necessary the spectra were corrected for possible inaccuracies in the sample thickness. The corrections were done on the premise that in the fully isotropic state, i.e. above the isotropic transition at 60°C (cf. figure 10), the contribution of the LC matrix to the static dielectric constant ε_s' of the colloidal mixtures should match $\varepsilon_{s,\mathrm{iso}}'$ of pure E7.

In order to calculate the value of $\varepsilon_{s,\mathrm{iso}}'$ for the LC matrix of the colloidal mixtures, a rule of mixtures for heterogeneous two-phase systems known as the generalized Looyenga equation [29] was used†:

$$\varepsilon^{*1-2n} = \phi_f \varepsilon_f^{*1-2n} + \phi_m \varepsilon_m^{*1-2n} \quad (4)$$

where ε^*, ε_f^* and ε_m^* represent the complex dielectric constant of the mixture, the filler particles and the continuous matrix (LC E7), respectively, ϕ_f and ϕ_m the volume fractions of the filler particles and the matrix material, respectively and n the shape or depolarization factor of the dispersed phase ($n = 1/3$ for spherical particles)‡. [In view of the aggregation of the colloidal particles into a network, a lower value than 1/3 might be chosen for $1-2n$ in equation (4), e.g. $1-2n = 1/5$.] For ε_m^* we substituted ε_z^* from equation (1), which simplifies to $\varepsilon_{iso}' = (\varepsilon_\parallel^* + 2\varepsilon_\perp^*)/3$ above the isotropic transition. We further used in equation (4) the low frequency

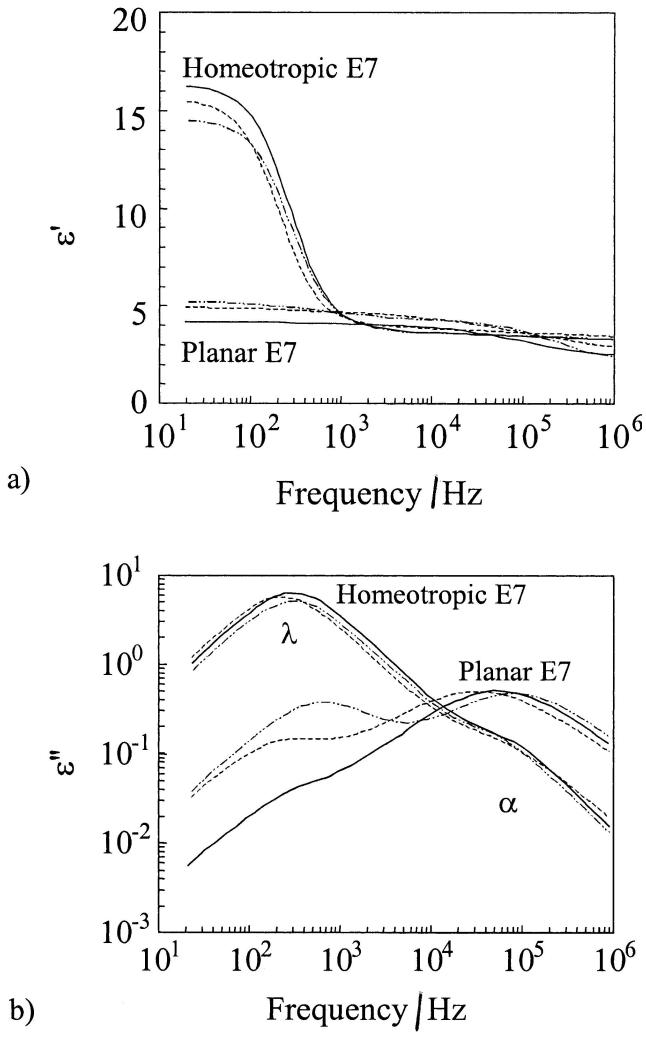

Figure 3. Havriliak–Negami fits of (*a*) the permittivity ε' and (*b*) the dielectric loss ε'' measured as a function of frequency at $T = -40^\circ$C for E7/colloid mixtures with varying colloid content: (—) 0 wt % (pure E7); (- -) 2.7 wt %; (—··) 6.4 wt %. For a fair comparison between the spectra, the ε'-curves of the mixtures were normalised to $\varepsilon_{s,\mathrm{iso}}'$ of pure E7.

†Looyenga's equation is based on the so-called differential approach. Another equation that can be used, up to reasonable volume fractions, is Maxwell–Garnett's mean-field formula [30–32]. This reads for spherical particles:

$$\varepsilon^* = \varepsilon_m^* \frac{\varepsilon_f^* + 2\varepsilon_m^* + 2\phi_f(\varepsilon_f^* - \varepsilon_m^*)}{\varepsilon_f^* + 2\varepsilon_m^* - \phi_f(\varepsilon_f^* - \varepsilon_m^*)}. \quad (4\,a)$$

‡Regarding the calculation of ε' and ε'' from mixture formulae like equation (4), we should realize that the dielectric losses are often rather small, so that $\varepsilon'' < \varepsilon'$. We might then use the following approximations: $\varepsilon'^{1-2n} \simeq \phi_f \varepsilon_f'^{1-2n} + \phi_m \varepsilon_m'^{1-2n}$ and $\varepsilon''/\varepsilon'^{2n} \simeq \phi_f \varepsilon_f''/\varepsilon_f'^{2n} + \phi_m \varepsilon_m''/\varepsilon_m'^{2n}$. Usually, such approximations are not necessary, as most computer programs can handle complex data directly.

data, in order to find the static value of ε'_{iso}. The volume fractions were approximated by their corresponding weight fractions, since the densities of both phases are approximately equal. For the crosslinked PMMA colloids a frequency-independent dielectric permittivity ε'_f of 3.5 was assumed. It is after correction of any thickness inaccuracy that we calculated the LC contribution ε^*_m for the colloid-LC mixtures samples using equation (4); this gives $\varepsilon^*_m = (\varepsilon^* - \phi_f \varepsilon'^{1/3}_f / 1 - \phi_f)^3$. In principle ε^*_m should equal ε^*_z in equation (3) and this enables us to find via equation (3) the order parameter S_d.

For a quantitative analysis of the spectra we have fitted the measured frequency dependence of $\varepsilon'(f)$ and $\varepsilon''(f)$ of the samples by a sum of two Havriliak–Negami (HN) relaxation functions [33], in order to account for the two relaxation processes α and λ:

$$\varepsilon'(\omega, T) = \varepsilon_\infty + \sum_{k=1}^{2} \mathscr{R}\left\{\frac{\Delta\varepsilon_k}{[1 + (i\omega\tau_k)^{a_k}]^{b_k}}\right\} \qquad (5)$$

$$\varepsilon''(\omega, T) = \sum_{k=1}^{2} \mathscr{T}\left\{\frac{\Delta\varepsilon_k}{[1 + (i\omega\tau_k)^{a_k}]^{b_k}}\right\} + \frac{\sigma}{\varepsilon_0 \omega} \qquad (6)$$

In equations (5) and (6), $\Delta\varepsilon_k$, τ_k, a_k and b_k denote the relaxation strengths, the relaxation times and the shape parameters a and b, respectively; $\mathscr{R}$ indicates the real part and $\mathscr{T}$ the imaginary part. The 2nd term in equation (6) represents the loss due to the ohmic conduction σ, which is small at low temperatures. Note that the parameters will depend on the filler fraction. A major advantage of the fit procedure is that it allows one to obtain the static permittivity ε'_s from the sum $\varepsilon'_s = \varepsilon'_\infty + \Delta\varepsilon_1 + \Delta\varepsilon_2$ even for spectra that do not show a clear plateau of the permittivity at the lowest frequency; cf. figure 3(*a*). The fit results obtained from the data of figures 3(*a*) and 3(*b*) are listed in table 1, together with the order parameters S_d for five sample compositions. The ε'_z and ε''_z-spectra plotted for the two mixtures were obtained by calculating ε'_m and ε''_m using mixture equation (4), with $n = 1/3$. The spectra therefore represent those of E7 *confined* within the colloidal network in the absence and presence of a strong electric field. They clearly differ from those for p- and h-alignment of pure E7; notably the $\varepsilon'_\parallel$-values are smaller, whereas the $\varepsilon'_\perp$-values are larger. As a result the losses in the planar state also become higher.

The results displayed in table 1 indicate that the colloidal dispersions obviously show a switching effect between the *unaddressed* (p-aligned) state and the *addressed* (h-aligned) state. As could be expected, the E7 becomes less perfectly oriented with increasing colloid content in both orientational states, due to local perturbation of the orientational ordering of the LC molecules that are in the proximity of the colloidal particles. Thus, with increasing colloid content the multidomain formation of the confined E7 becomes more significant. The variation in director order with blend composition is nicely illustrated via a change in the ratio of the relaxation strengths of the α and λ peak; see figure 3(*b*) and table 1.

3.2.2. *The three-phase interlayer model*

For E7 in the isotropic phase, the continuous LC medium and the LC molecules in the direct neighbourhood of the inclusions both adopt a random orientation. In this situation, a two-phase model, such as the two-component Looyenga model [29, 34], is sufficiently adequate to describe the dielectric properties of the heterogeneous material. However, in the *nematic* state of the liquid crystal *three* distinct phases with different dielectric permittivities should be considered: (i) the crosslinked colloids as the dispersed phase, (ii) the aligned, 'free' LC as the continuous bulk medium and, additionally, (iii) a *shell* around the particles consisting of LC molecules with a distorted orientation. To this situation, the so-called interlayer model, which uses the asymmetrical mean-field approach, should be applied. This model accounts for the presence of an additional interfacial layer in matrix-inclusion type heterogeneous materials (figure 4) [32, 35].

The interlayer model describes the dielectric behaviour of a 'core–shell' mixture as follows:

$$\varepsilon^* = \frac{\varepsilon^*_f \phi_f + \varepsilon^*_l \phi_l X^* + \varepsilon^*_m \phi_m Z^*}{\phi_f + \phi_l X^* + \phi_m Z^*} \qquad (7)$$

Table 1. Director order parameters (S_d) and dielectric strength from fits of the α- and λ-peaks for E7 with a varying colloid content in the unaddressed (0 V) and addressed (40 V) states. S_d applies to the lowest frequency of 20 Hz.

					S_d	
Colloid content/wt %	$\Delta\varepsilon_\perp(\lambda)$ 0 V	$\Delta\varepsilon_\perp(\alpha)$ 0 V	$\Delta\varepsilon_\parallel(\lambda)$ 40 V	$\Delta\varepsilon_\parallel(\alpha)$ 40 V	0 V	40 V
0 (E7)	0.050	1.37	12.9	0.173	−0.50	1.00
2.7	0.248	1.42	11.6	0.226	−0.40	0.93
4.5	0.565	1.32	—	—	−0.40	—
6.4	0.771	1.19	10.5	0.176	−0.38	0.79
8.6	0.540	1.19	—	—	−0.39	—

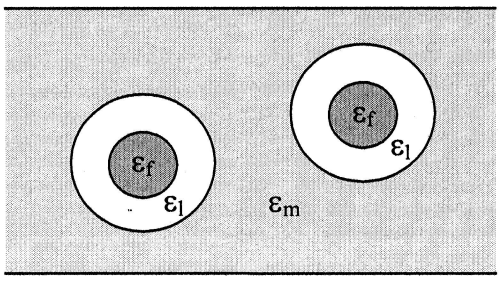

Figure 4. Representation of a nematic LC E7 matrix, filled with colloidal particles according to the three-phase interlayer model. The interfacial layer is made up of LC molecules with a random orientation, confined within a shell around the particles.

with:

$$X^* = \frac{[n\varepsilon_f^* + (1-n)\varepsilon_l^*]}{\varepsilon_l^*} \tag{8}$$

$$Z^* = \frac{[n\varepsilon_f^* + (1-n)\varepsilon_l^*][n\varepsilon_l^* + (1-n)\varepsilon_m^*] + vn(1-n)(\varepsilon_f^* - \varepsilon_l^*)(\varepsilon_l^* - \varepsilon_m^*)}{\varepsilon_l^* \varepsilon_m^*} \tag{9}$$

$$v = \frac{\phi_f}{\phi_f + \phi_l} \tag{10}$$

where ε_l^* and ϕ_l are, respectively, the complex dielectric constant and volume fraction of the interfacial layer. The *static* dielectric constants of figure 3(*a*) were modelled with equation (7), taking $n = 1/3$ and using ϕ_l as the fit variable§. For ε_l' we took the isotropic dielectric constant of E7, ε_{iso}' given earlier $\varepsilon_{iso}' = (\varepsilon_\parallel' + 2\varepsilon_\perp')/3$ [27]. The values for $\varepsilon_\parallel'$ and $\varepsilon_\perp'$ in $\varepsilon_z' = \varepsilon_m'$ were taken from the fits of the experimental curves for h- and p-aligned E7. For the colloid-filled LC samples the thickness of the interfacial layer, D_1, was found from the calculated volume fraction $\phi_l(D_1/r_f = [1 + \phi_f/\phi_l]^{1/3} - 1$, with r_f the radius of the filler particles). The results are listed in table 2 for the samples containing various amounts of colloids¶.

§We can eliminate X^* and Z^* from equation (7); we then obtain for a mixture of spherical particles ($n = 1/3$) with a shell:

$$\frac{\varepsilon^* - \varepsilon_m^*}{\varepsilon^* + 2\varepsilon_m^*} = p\frac{[(\varepsilon_f^* + 2\varepsilon_l^*)(\varepsilon_m^* - \varepsilon_l^*) - v(\varepsilon_f^* - \varepsilon_l^*)(\varepsilon_m^* + 2\varepsilon_l^*)]}{(\varepsilon_f^* + 2\varepsilon_l^*)(2\varepsilon_m^* + \varepsilon_l^*) - 2v(\varepsilon_f^* - \varepsilon_l^*)(\varepsilon_m^* - \varepsilon_l^*)} \tag{7a}$$

where $p = \phi_f + \phi_l$. After substituting the static values for the permittivities, both expressions yield a quadratic equation for ϕ_l with one positive root.

¶Looyenga's model, which is symmetrical regarding the various components, can of course also be extended to three phases. It then adds up to: $\varepsilon^{*1/3} = \phi_f\varepsilon_f^{*1/3} + \phi_l\varepsilon_l^{*1/3} + \phi_m\varepsilon_m^{*1/3}$. The results hardly differ from those obtained with equation (7). Even the simple additive mixture rule: $\varepsilon^* = \phi_f\varepsilon_f^* + \phi_l\varepsilon_l^* + \phi_m\varepsilon_m^*$ holds quite well, because the filler volume fractions are rather low. This is interesting since these equations give explicit expressions for ϕ_l and ε_m and are therefore easier to use than equation (7).

Table 2. Volume fraction and thickness of the isotropic shell around the colloidal particles according to the interlayer model. The calculations are based on the static dielectric constant of colloid/E7 mixtures in the unaddressed and addressed states. The calculations show that the layer thickness decreases with increasing voltage.

	ϕ_l		D_1/nm	
ϕ_f	0 V	40 V	0 V	40 V
0.027	0.208	0.070	326	164
0.045	0.220	—	254	—
0.064	0.231	0.150	209	156
0.086	0.180	—	144	—

The decrease in the interfacial layer thickness suggests that agglomeration phenomena become more significant with increasing colloid content in the E7. The remaining shell of perturbed LC after application of a bias voltage is indicative of the incomplete homeotropic alignment of the LC.

3.2.3. *Quasi-static field-induced changes of the director order and their effect on the dielectric spectra*

Whereas the previous sections were focused on the ultimate planar and homeotropic order achievable in E7 and the related colloidal mixtures, we now want to discuss the switching process from the initial planar 'off'-state to the homeotropically aligned 'on'-state in more detail. For this purpose, dielectric spectra were taken while the samples were subjected to a d.c. voltage in order to ensure a quasi-static state of alignment during the acquisition of an individual spectrum. By step-wise increase in the d.c. bias from 0 to 40 V, a gradual change from p-alignment to h-alignment was induced, which resulted in marked changes in the dielectric spectra as shown in figures 5(*a–f*). Upon increasing the bias voltage, all materials display a competitive behaviour between the height of the λ-relaxation peak (gradually increasing) and the height of the α-peak (gradually decreasing).

Figures 5(*a*) and 5(*b*) show a striking feature of pure E7, the existence of two isosbestic†† or crossover points, i.e. frequencies at which either ε' or ε'' become equal and independent of the state of alignment S_d; cf. equation (1) for $\varepsilon_\parallel' = \varepsilon_\perp'$ or $\varepsilon_\parallel'' = \varepsilon_\perp''$. Upon addition of colloids to the E7, these isosbestic points become less obvious or even disappear as the λ-relaxation peak gradually shifts with increasing bias voltage. The vanishing of the isosbestic points is strong evidence for a complex, heterogeneous dielectric material. This phenomenon will be addressed further in the next section.

For a quantitative analysis, the ε' and ε'' spectra were fitted to equations (5) and (6). The results are displayed

††Sbesis (Gr.) means extinction.

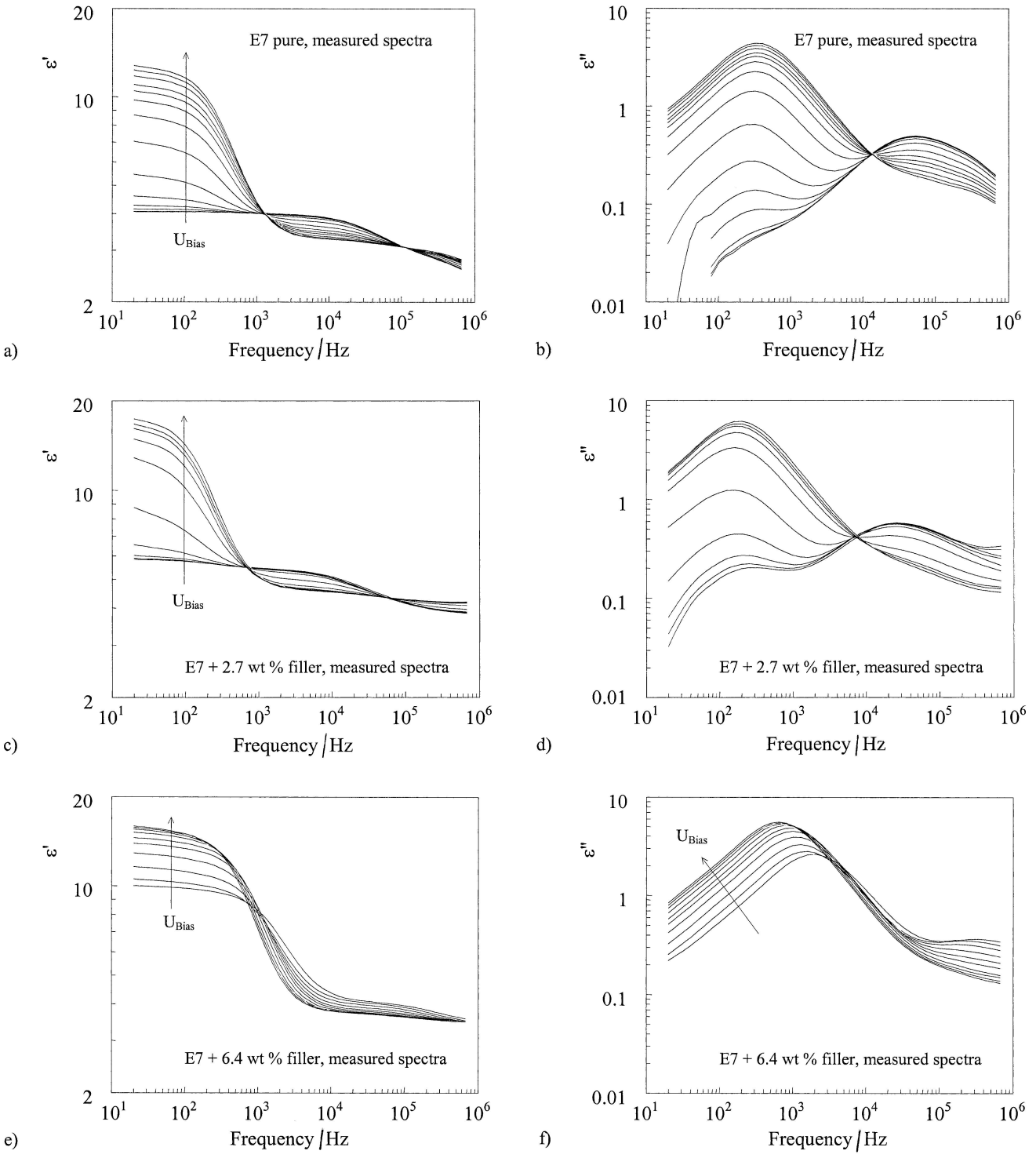

Figure 5. Dielectric spectra of E7/colloid mixtures with varying colloid content: (*a*, *b*) 0 wt % (pure E7); (*c*, *d*) 2.7 wt %; (*e*, *f*) 6.4 wt %. The spectra were collected at $-40°C$ during the application of a bias voltage, which was gradually increased from 0 to 40 V (E7: $\Delta V = 0.25$ V; 2.7 and 6.4 wt % colloids/E7: $\Delta V = 2$ V). In particular, for 6.4 wt % the spectra differ markedly from those of pure E7.

in figures 6 and 7 showing the relaxation strengths $\Delta\varepsilon_\alpha$ and $\Delta\varepsilon_\lambda$ as well as the corresponding relaxation times τ_α and τ_λ.

Figure 6 shows the (quasi-static) switching characteristics in terms of a field-dependent relaxation strength, which is manifested in both $\Delta\varepsilon_\alpha$ and $\Delta\varepsilon_\lambda$. Surprisingly,

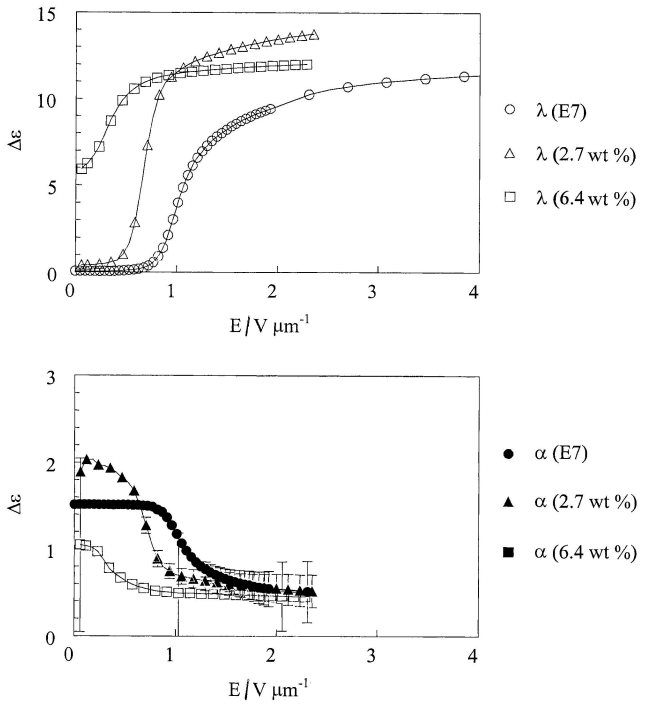

Figure 6. Dielectric relaxation strength $\Delta\varepsilon$ of the α- and λ-processes for E7 and E7/colloid mixtures obtained from fits to the dielectric spectra in figure 5 at -40°C as a function of the bias field. For pure E7 and 2.7 wt % $\Delta\varepsilon_{\lambda}$ is negligible at 0 V μm^{-1} (≈ 0.055). This is no longer so for 6.4 wt %, because the planar alignment, being distorted by anchoring, has not yet been fully restored.

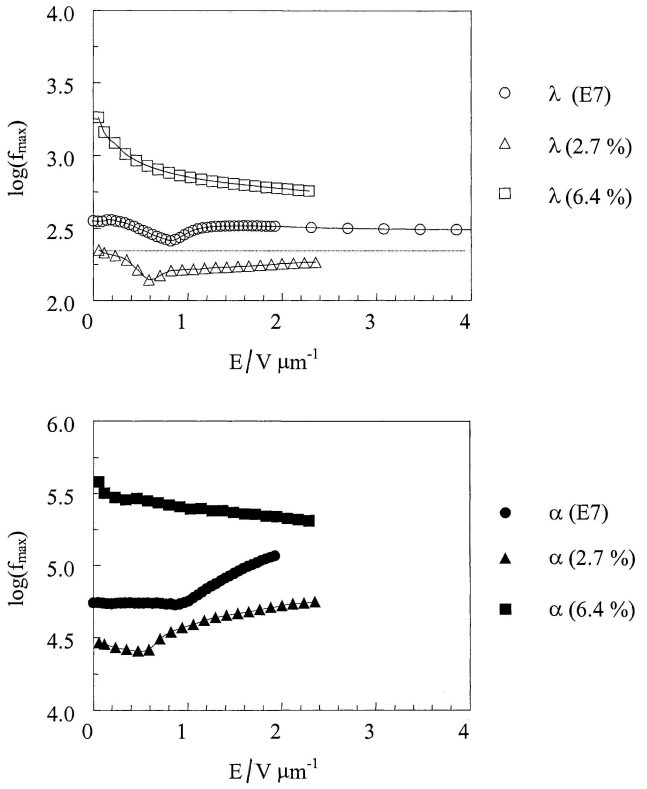

Figure 7. Change in peak relaxation frequency f_{max} with bias field for the α- and λ-processes of E7 and E7/colloid mixtures obtained from the shift of the dielectric loss spectra of figure 5 at -40°C.

the pure liquid crystal exhibits the highest threshold field. Addition of 2.7 wt % of colloidal filler results in a lowering of the threshold field, while maintaining the switching range between full p- and h-alignment. Further increase of the filler content reduces the threshold field even more. However, then no recovery to the p-aligned state occurs at -40°C on the time scale of the experiment, as is evident from $\Delta\varepsilon_{\lambda}$ at $E = 0$ for 6.4 wt %.

The reduction of the threshold field upon addition of a second phase to an LC has been described earlier for anisotropic thermo-reversible gels in TN cells [36]. For colloidal fillers such strong effects have not been reported before, although previous electro-optical experiments indicated a slight reduction of the threshold field at high filler contents [19]. However, those experiments were done at room temperature, whereas the present dielectric switching experiments are carried out at a rather uncommonly low temperature. A possible explanation for the reduction of the threshold field could be sought in the anchoring of the LC domains to the colloidal network. This anchoring interaction will (locally) dominate over the interaction between the LC and the rubbed polyimide layers, resulting in elastic director deformations. As a consequence, parts of the domains are able to switch between *two metastable* orientational states, which might lower the elastic energy to be overcome by the electric field. In addition, local field enhancements due to the dielectric heterogeneities are also likely to contribute to the low-field switching characteristics.

For E7, we have calculated the director order parameter S_d on the basis of the field-dependent relaxation strengths $\Delta\varepsilon_{\alpha}$ and $\Delta\varepsilon_{\lambda}$. By applying equation (1) at $\omega \to 0$ and $\omega \to \infty$, and denoting $\Delta\varepsilon = \varepsilon_{\omega\to 0} - \varepsilon_{\omega\to\infty}$ (cf. figure 2) we find:

$$S_d(\Delta\varepsilon_{\lambda}) = \frac{3\Delta\varepsilon_{\lambda} - \Delta\varepsilon_{\lambda\parallel} - 2\Delta\varepsilon_{\lambda\perp}}{2(\Delta\varepsilon_{\lambda\parallel} - \Delta\varepsilon_{\lambda\perp})} \tag{11}$$

and

$$S_d(\Delta\varepsilon_{\alpha}) = \frac{3\Delta\varepsilon_{\alpha} - \Delta\varepsilon_{\alpha\parallel} - 2\Delta\varepsilon_{\alpha\perp}}{2(\Delta\varepsilon_{\alpha\parallel} - \Delta\varepsilon_{\alpha\perp})}. \tag{12}$$

Equations (11) and (12) (which can also be derived from equation (15) below) represent an alternative to equation (3) for the determination of S_d from each of the two processes contributing to the dielectric spectrum according to figure 2. Consequently, both equations should yield the same S_d value, as is demonstrated for pure E7 in figure 8.

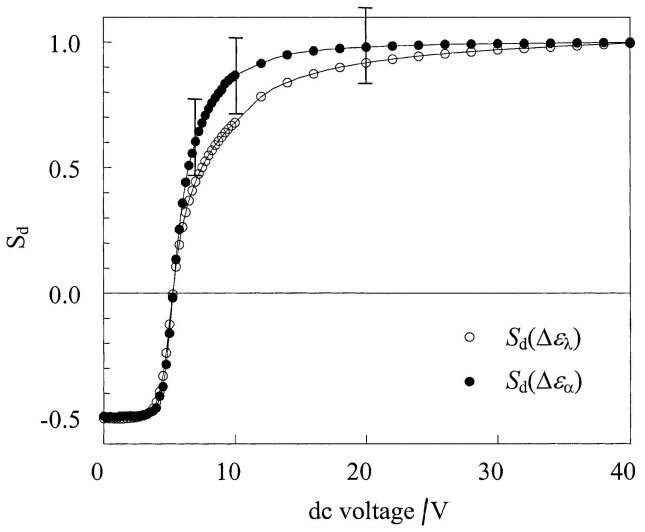

Figure 8. Director order parameter S_d vs. bias voltage calculated from the relaxation strengths $\Delta\varepsilon_\alpha$ and $\Delta\varepsilon_\lambda$ using equations (11) and (12).

From figure 8 we see that both $S_d(\Delta\varepsilon_\alpha)$ and $S_d(\Delta\varepsilon_\lambda)$ almost coincide in the S_d-range from -0.5 to 0.2, while the curves deviate in the homeotropic region. This discrepancy can be attributed to larger inaccuracies in $\Delta\varepsilon_\alpha$ indicated by the error bars given in figure 6 (*b*).

3.2.4. *Modelling of field-induced orientational behaviour of pure LC and LC confined within a colloidal network*

In addition to the relaxation strength, which yields the (mean) director order parameter, the fits also provide accurate information about the time scale of the molecular relaxations, expressed by the relaxation times of the two principal relaxations τ_α and τ_λ (cf. figure 7). The slow λ-relaxation is very *typical* of LC molecules and is related to the tumbling of the rod-like LC molecules over their short axes, which can be described fairly well with a single-relaxation time process (Debye relaxation)‡‡. In contrast, the fast α-process is the manifestation of virtually indistinct rotations about the long axis and a precessional motion about the director. This combination causes peak broadening and an average relaxation time, which depend on the angle between the electric field and the nematic director [37]. We will restrict ourselves to the λ-process.

According to figure 7, the peak relaxation frequency of pure E7, f_λ (which is determined by the relaxation time τ_λ, since $2\pi f_\lambda \tau_\lambda = 1$ for symmetric peaks) shows indeed only a marginal dependence on the state of alignment. The small local minimum corresponds to the transition range between p- and h-alignment, where a planarly-aligned surface layer coexists with an oriented bulk fraction, possibly causing a slight peak shift due to the dielectric inhomogeneity in that transition region. However, much larger peak shifts are found for the colloidal mixtures, which forces us to seek for alternative explanations.

In order to decide whether the peak shifts are exclusively caused by the dielectric heterogeneity or reflect intrinsic changes of the molecular relaxation times, we have performed model calculations. For convenience we will first assume two single-relaxation time processes (Debye relaxations) and an order parameter-dependent high-frequency dielectric constant ε_∞. For the real part we get two expressions, describing the h- and p-aligned case:

$$\varepsilon'_\parallel(\omega) = \varepsilon'_{\infty\parallel} + \frac{\Delta\varepsilon_{\lambda\parallel}}{1+\omega^2\tau_\lambda^2} + \frac{\Delta\varepsilon_{\alpha\parallel}}{1+\omega^2\tau_\alpha^2} \tag{13}$$

and

$$\varepsilon'_\perp(\omega) = \varepsilon'_{\infty\perp} + \frac{\Delta\varepsilon_{\lambda\perp}}{1+\omega^2\tau_\lambda^2} + \frac{\Delta\varepsilon_{\alpha\perp}}{1+\omega^2\tau_\alpha^2}. \tag{14}$$

Combining these relations with equation (1) yields

$$\varepsilon'_z(\omega) = \left[\varepsilon'_{\infty\parallel} + \frac{\Delta\varepsilon_{\lambda\parallel}}{1+\omega^2\tau_\lambda^2} + \frac{\Delta\varepsilon_{\alpha\parallel}}{1+\omega^2\tau_\alpha^2}\right]\frac{1+2S_d}{3} + 2\left[\varepsilon'_{\infty\perp} + \frac{\Delta\varepsilon_{\lambda\perp}}{1+\omega^2\tau_\lambda^2} + \frac{\Delta\varepsilon_{\alpha\perp}}{1+\omega^2\tau_\alpha^2}\right]\frac{1-S_d}{3}. \tag{15}$$

The corresponding loss reads

$$\varepsilon''_z(\omega) = \left[\frac{\Delta\varepsilon_{\lambda\parallel}\omega\tau}{1+\omega^2\tau_\lambda^2} + \frac{\Delta\varepsilon_{\alpha\parallel}\omega\tau}{1+\omega^2\tau_\alpha^2}\right]\frac{1+2S_d}{3} + 2\left[\frac{\Delta\varepsilon_{\lambda\perp}\omega\tau}{1+\omega^2\tau_\lambda^2} + \frac{\Delta\varepsilon_{\alpha\perp}\omega\tau}{1+\omega^2\tau_\alpha^2}\right]\frac{1-S_d}{3}. \tag{16}$$

Actually, we should include the conduction loss in equation (16), but this can be neglected at low temperatures.

Figure 9 displays a set of spectra generated with equations (15) and (16), using realistic values for $\Delta\varepsilon_{\lambda\perp}$, $\Delta\varepsilon_{\lambda\parallel}$, $\Delta\varepsilon_{\alpha\perp}$, $\Delta\varepsilon_{\alpha\parallel}$, $\varepsilon_{\infty\perp}$, $\varepsilon_{\infty\parallel}$, τ_λ and τ_α obtained from the fit of measured E7 spectra. By comparing the computed spectra of figures 9 (*a*) and 9 (*b*) with those measured for pure E7, figures 5 (*a*) and 5 (*b*), we see that the modelled spectra agree very well with the experimental curves,

‡‡The notation λ (Gr.1) accentuates that this slow end-over-end reorientation is characteristic for liquid crystals with their long, rod-like molecules. In the literature it is often called δ-relaxation, but this notation might imply that it is faster than the α-relaxation, which is *not* true. The α-relaxation has not been renamed, because this relaxation is common for all types of molecule. It is also the latter that is frozen-in at the glass transition upon cooling, whereas the slow λ-relaxation is already immobilized at a temperature above the glass transition temperature.

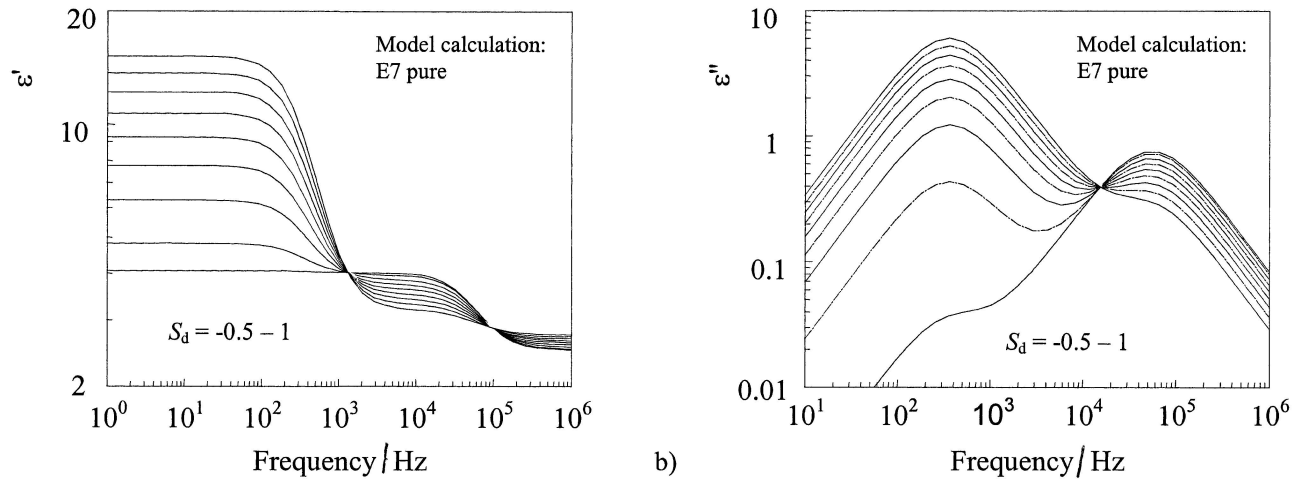

Figure 9. Modelling of the dielectric spectra of pure E7 (*a*, *b*) and a 6.4 wt % colloidal mixture (*c*, *d*) as a function of the director order parameter of the matrix LC phase using the parameters: (*a*, *b*) $\Delta\varepsilon_{\lambda\perp} = 0.055$, $\Delta\varepsilon_{\lambda\parallel} = 12.0$, $\Delta\varepsilon_{\alpha\perp} = 1.52$, $\Delta\varepsilon_{\alpha\parallel} = 0.45$, $\varepsilon_{\infty\perp} = 2.5$, $\varepsilon_{\infty\parallel} = 2.75$, $\tau_\lambda = 4.47 \times 10^{-4}$ s, $\tau_\alpha = 2.88 \times 10^{-6}$ s; (*c*, *d*) $\Delta\varepsilon_{\lambda\perp} = 3.5$, $\Delta\varepsilon_{\lambda\parallel} = 12.0$, $\Delta\varepsilon_{\alpha\perp} = 1.52$, $\Delta\varepsilon_{\alpha\parallel} = 0.45$, $\varepsilon_{\infty\perp} = 2.5$, $\varepsilon_{\infty\parallel} = 2.75$, $\tau_\lambda = 4.47 \times 10^{-4}$ s, $\tau_\alpha = 2.88 \times 10^{-6}$ s. Note that ϕ_l was assumed to decrease with S_d, cf. equation (18). Furthermore, the relaxation times of the isotropic LC phase contained in ϕ_l were assumed to be shorter than τ_λ and τ_α, viz. $\tau_{\lambda,iso} = 8 \times 10^{-5}$ s and $\tau_{\alpha,iso} = 4 \times 10^{-7}$ s.

even quantitatively. Since the model assumes a homogeneous LC material, no peak shifts were found in the computed loss spectra for E7.

As a next step we tried to model the more complex behaviour of the colloidal mixture of E7 with 6.4 wt % of filler, the measured spectra of which are given in figures 5(*e*) and 5(*f*). For this purpose we had to use a rule of mixtures, in order to account for the existence of a bulk LC phase and a filler-associated, isotropic LC phase. Although the *interlayer* model, equations (7–10), would be more appropriate, we have chosen the Looyenga equation because it is easier to implement. This gives, for example, for ε' the expression

$$\varepsilon'^{1/3}(\omega, S_d) \simeq \phi_f \varepsilon_f'^{1/3} + \phi_l \varepsilon_{z,iso}'^{1/3}(\omega) + \phi_m \varepsilon_z'^{1/3}(\omega, S_d). \quad (17)$$

The frequency dependent term $\varepsilon_z'(\omega, S_d)$ follows from equation (15); the same applies to the isotropic permittivity $\varepsilon_{z,iso}'(\omega)$ of the interlayer, for which $S_d = 0$.

It emerged that equation (17) could simulate neither a peak shift nor the disappearance of the isosbestic points as shown in figures 5(*e*) and 5(*f*). Therefore we have tried, in line with the change in D_1 in table 2, to link the value of the varying, isotropic layer fraction ϕ_l to the director order parameter of the bulk phase, in a similar way to the permittivity changes with S_d according to equation (3):

$$\frac{\phi_l(S_d) - \phi_l(S_d = 0)}{\phi_l(S_d = 1) - \phi_l(S_d = -.5)} = \frac{2S_d}{3}. \quad (18)$$

Equation (18) enables the adjustment of ϕ_l to the applied d.c. bias, since for high voltages $S_d \to 1$, while for zero bias $S_d \to -1/2$.

This extension of the model, whereby $\phi_l(S_d)$ was substituted for ϕ_l in mixture formula (17) did not lead to a greatly improved fit between the computed and the experimental spectra. More particularly, no significant shift in the loss peaks with variation in S_d and $\phi_l(S_d)$, as seen in figure 5(*f*), was achieved. This led us to the conclusion that the change in relaxation times present in colloidal mixtures must be *intrinsic*. Consequently, we had to take into account that the bulk phase and the isotropic fraction of LC E7 have *different* relaxation times, which was already suggested by the results displayed in figure 7. By inserting in equations (15–17), larger relaxation times for the bulk fraction ($\tau_{\alpha,bulk}$, $\tau_{\lambda,bulk}$) and smaller for the more mobile, voltage-dependent near-filler fraction ($\tau_{\alpha,iso}$, $\tau_{\lambda,iso}$), we were able to obtain reasonable agreement with the experimental behaviour of E7 with 6.4 wt % filler. The simulated spectra are shown in figures 9(*c*) and 9(*d*). They reveal both an absence of the isosbestic points and, qualitatively, a remarkable shift in the λ-peak upon switching between p- and h-alignment. Although this final model is still an aproximation for the complex situation present in liquid crystals dispersed in a colloidal network, it provides sufficient support for the fact that different LC fractions with specific molecular mobilities exist in such materials. One possible molecular reason for altering the molecular dynamics could be the change in anchoring from a weak to a strong anchoring regime affecting particularly the mobility near internal surfaces [11–13, 38]. In addition, changes in the relaxation time of the λ-process are also likely to occur as a result of elastic director deformations in the LC domains. More experiments and theoretical work are necessary for a detailed understanding of these effects§§.

§§ Perhaps more attention should be paid to the *clustering* of the particles. This could be achieved by a two-step modelling of the mixtures. In the first step the permittivity within a cluster is calculated by envisaging that a shell of isotropic LC surrounds the filler particles. We then have from equation (4 *a*):

$$\varepsilon_{fl}^* = \varepsilon_l^* \frac{\varepsilon_f^* + 2\varepsilon_l^* + 2\phi_f(\varepsilon_f^* - \varepsilon_l^*)/(\phi_f + \phi_l)}{\varepsilon_f^* + 2\varepsilon_l^* - \phi_f(\varepsilon_f^* - \varepsilon_l^*)/(\phi_f + \phi_l)}$$

in which we should substitute $\varepsilon_l^* = \varepsilon_{z,iso}^*(\omega)$ and $\phi_l = f(\text{bias}) = f(S_d)$ given earlier. Next, the permittivity of the clusters and the nematic LC matrix is modelled with equation (4), in which n will depend on the aspect ratio of the clusters. This second step leads to a final ε^* for the aggregated colloid-LC mixture of:

$$\varepsilon^{*1-2n} = (\phi_f + \phi_l)\varepsilon_{fl}^{*1-2n} + \phi_m \varepsilon_m^{*1-2n}$$

where $\varepsilon_m^* = \varepsilon_z^*(\omega, S_d)$. Such a two-step approach has been suggested earlier for flocculated emulsions [31].

3.2.5. *Temperature- and time-dependent switching of the director order in pure LC*

The temperature-dependent alignment of the LC E7 is illustrated in figure 10. The figure shows the initial permittivities of E7 in the planarly-aligned state together with the permittivities that were collected at the end of a voltage step from 0 to 40 V, as a function of temperature and at a frequency of 1 kHz. At temperatures above ~60°C, E7 is in the isotropic phase and no longer aligns in a d.c. field. As expected, at temperatures well below −40°C (which approach the glass transition of E7 at −65°C) again no response is observed, indicating that the molecular motions (of both the α- and λ-processes) are frozen-in.

The time-dependence of the orientational behaviour of E7 was investigated by subjecting the LC sample to a step-voltage sequence $0 \to 40 \to 0$ V (see figure 11), where each voltage level was maintained for 2 min. In this way, the retardation behaviour to the homeotropic state, driven by the electric field, and the recovery behaviour of the nematic director to the planar (ground or off) state, controlled by elastic restoration forces can be addressed separately. The step experiments were performed at temperatures ranging from 25 down to −50°C and at a fixed frequency of 110 Hz (figure 11). The time interval between the successive curves is 2 s.

Let us first focus on the switching to the 'on'-state. From figure 11 we see that (on the time-scale of the experiment) the LC material shows an almost instantaneous switching behaviour to the homeotropic state even for temperatures as low as −40°C. In contrast, the relaxation of the nematic director to the planar state, i.e. after removal of the bias voltage, shows a noticeable slow-down at both the highest and the lowest temperatures.

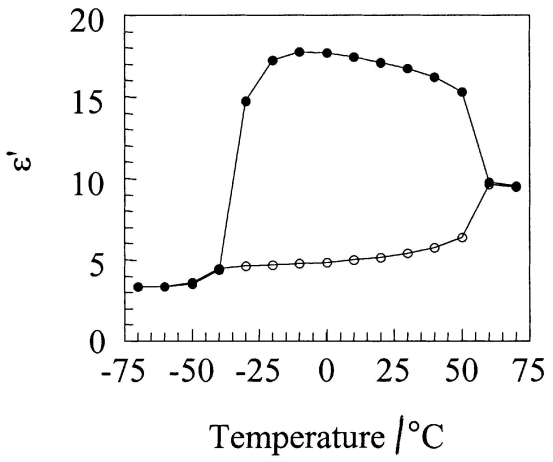

Figure 10. Dielectric permittivity as a function of temperature for pure E7 found by scanning at 1 kHz in the 0 V unaddressed state (○) and the 40 V addressed state (●). The nematic–isotropic transition at 60°C becomes clearly apparent in these curves.

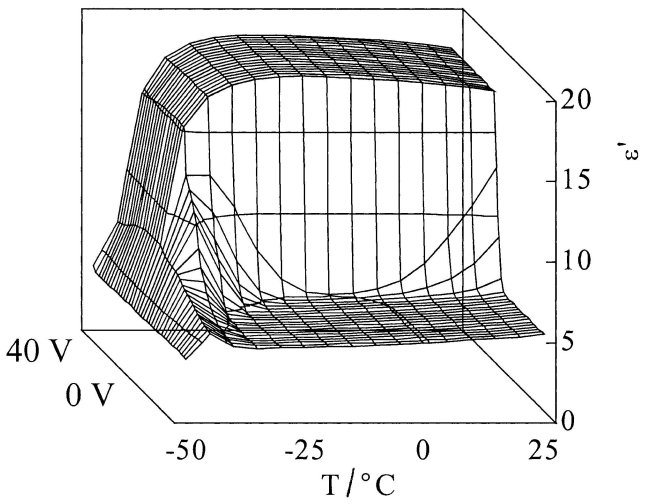

Figure 11. Change with time of the permittivity in the temperature region between 25 to -50°C for pure E7 measured at 110 Hz after switching to 40 V (addressed state—curves at the rear) and then 0 V (unaddressed state—curves at the front).

The increasing relaxation time for the decay of the nematic order with decreasing temperature is plausible since the restoration of the planar order is directly linked to the viscosity of the nematic crystal, which in turn scales with the relaxation times of the two principal molecular relaxations [39]. Hence, only at sufficiently high temperatures do we find an instantaneous decay of the nematic order on the time scale of our experiment.

The delayed relaxation behaviour in the high temperature range is obviously of a different nature, most likely associated with an increase in conductivity as ionic impurities start to respond to the biasing d.c. field. This effect is well known from dielectric liquids as electrode polarization, caused by accumulation of ionic charges at the ion-blocking liquid/electrode interface. In this way, an internal field is built up with a time constant τ_{EP} (EP: electrode polarization) which is given by the cell bulk resistance, R, and the two double layer capacitances, C_d, in series to R according to $\tau_{EP} = RC_d/2$. A more detailed treatment of this effect is given elsewhere [40].

Electrode polarization can easily be identified in the frequency spectra $\varepsilon'(f)$ as a huge increase in the dielectric constant beyond the static permittivity of the LC. Since the time constant τ_{EP} usually also scales with the molecular relaxations, electrode polarization only manifests itself at elevated temperatures, if the time scale of the experiments approaches τ_{EP}. Upon addition of non-conductive particles of the LC, the ionic charges will also accumulate near the colloidal particles. This additional charging phenomenon is known as the Maxwell–Wagner effect [26, 41].

Summarizing the features seen in figure 11, one has to be aware that the switching characteristics reflect both molecular reorientation processes and electric field redistribution effects. This is demonstrated in three individual voltage ramp scans showing unusual hysteresis and memory effects; see figures 12 (*a–c*).

From figure 12 (*a*), corresponding to a triangular positive and negative voltage cycling experiment at 20°C, we recognize that the relaxation to the planar order occurs apparently at a higher d.c. voltage than is necessary for switching to the homeotropic state. In terms of elastically controlled relaxation of the director order this behaviour is counterintuitive. Clearly, the effective internal field over the bulk LC does not coincide with the applied external field, indicating the existance of a temporary internal field of opposite sign.

At a rather low temperature of -30°C the slow molecular dynamics leads to a reversion of the hysteresis, whereby the dielectric permittivity under decreasing voltage rises above the dielectric permittivity under increasing voltage, figure 12 (*c*). At an intermediate temperature of 0°C, both temperature-specific phenomena are absent and the voltage step-up scan coincides nicely with the voltage-down scan, figure 12 (*b*). In accordance with figure 11, it is emphasized that these hysteresis effects are also strongly time-dependent, especially at a low temperature of -30°C. This implies that the time span over which the voltage scan is applied also determines the magnitude of the hysteresis.

3.2.6. *Temperature- and time-dependent switching of the director order in LC confined within a colloidal network*

For the LC-colloidal dispersions the same experiments were performed as for the bulk E7. Figure 13 shows the

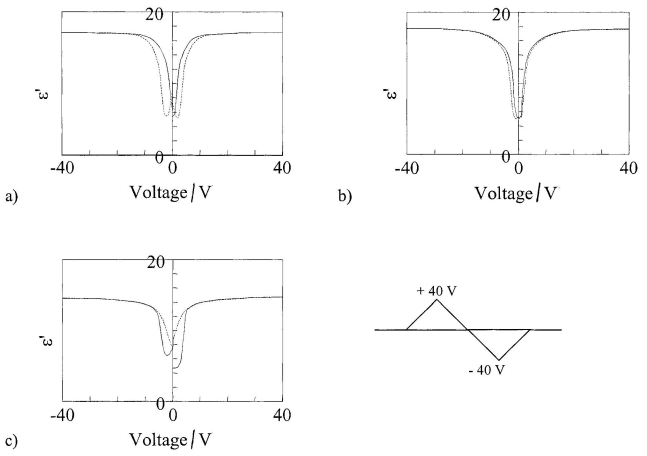

Figure 12. Triangular voltage-up (—) and -down (--) scans from 0 to ± 40 V showing the change in ε' for pure E7 at three temperatures: (*a*) 20, (*b*) 0, (*c*) -30°C.

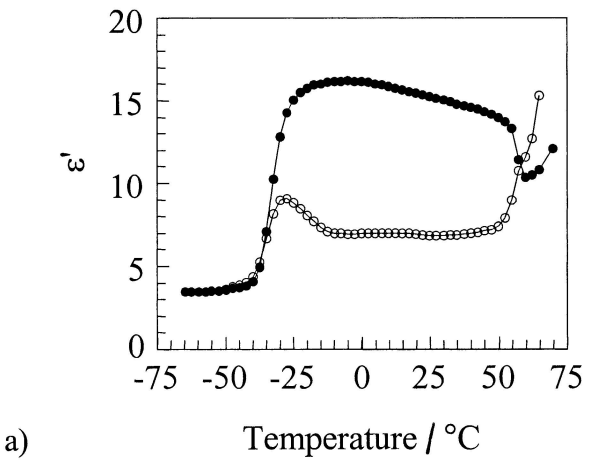

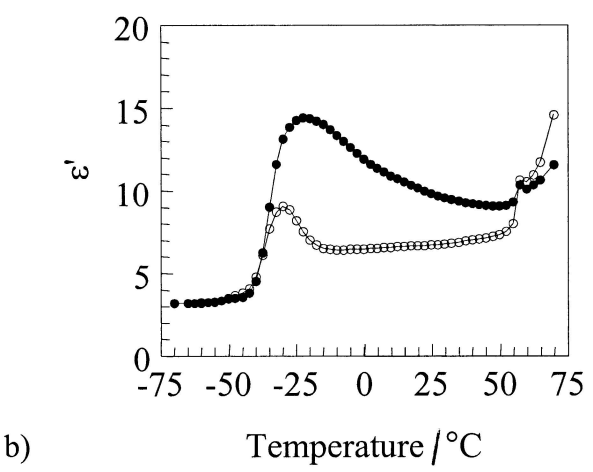

Figure 13. Permittivity as a function of temperature for (*a*) 2.7 wt % and (*b*) 6.4 wt % colloid/E7 samples scanned at 1 kHz in the 0 V unaddressed state (○) and the 40 V addressed state (●).

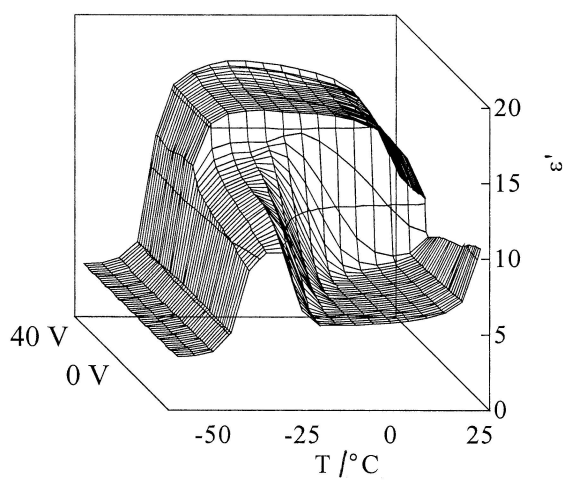

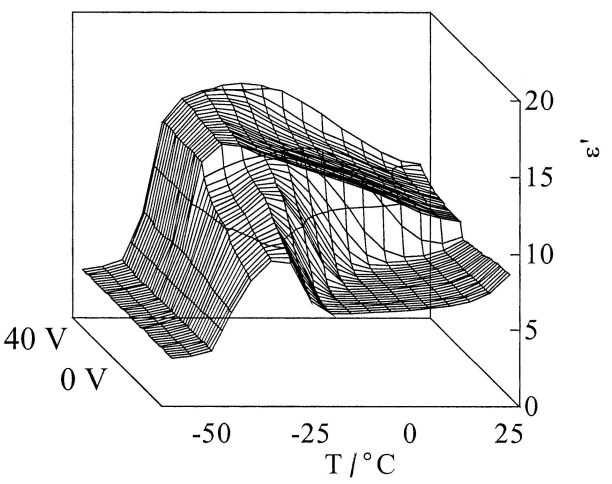

Figure 14. Change in permittivity in the temperature range from 25 to −60°C for (*a*) a 2.7 wt % and (*b*) a 6.4 wt % colloid/E7 sample measured at 110 Hz at time intervals of 2 s after switching to 40 V (addressed state—curves at the rear) and then to 0 V (unaddressed state—curves at the front).

permittivities of 2.7 and 6.4 wt % colloid/E7 samples as a function of temperature, in the unaddressed and addressed state. With increasing colloid content, less perfectly p- and h-aligned states are achieved. For the initial static dielectric constants an additional (remaining) orientation is visible at low temperatures. In the case of the highest filler content (6.4 wt %) the bias field applied is obviously too low to achieve effective homeotropic alignment of the E7 bulk fraction, due to the large cell thickness of 17.8 μm.

Figure 14 shows the retardation and relaxation behaviour of the (mean) nematic director as a response to a step-up ($0 \rightarrow 40$ V) and step-down ($40 \rightarrow 0$ V) bias change. For both colloidal mixtures, *two* distinct slow decay processes or relaxation phenomena can be identified at *low* temperatures instead of the sole decay process present in pure E7. While the low temperature decay process around −30°C corresponds closely to that of bulk E7, the other relaxation phenomenon around −10°C implies that charge phenomena could be involved in this odd decay response. This idea is supported by figure 14 (*b*) showing an overshoot in the permittivity around −10°C just after switching off the d.c. voltage, possibly indicating the presence of a strong internal field [42]. Another manifestation of an internal field is provided by hysteresis experiments using a triangular cycling voltage, the results of which are displayed in figures 15 (*a*) and 15 (*b*). Again, an 'abnormal' hysteresis is found very similar to that presented in figure 12 (*a*).

On the basis of the Maxwell–Wagner effect, it could be anticipated that the charge polarization effects become stronger upon addition of non-conductive colloids to

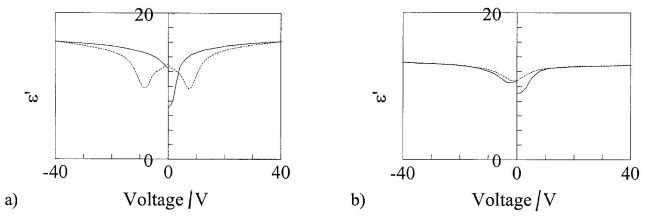

Figure 15. Triangular voltage-up (—) and -down (--) scans from 0 to ± 40 V depicted the variation in ε' for a 2.7 wt % colloidal dispersion in E7 at two temperatures: (*a*) 0, (*b*) -30°C.

the LC medium [26], and are present at lower temperatures for colloid-filled LC than for bulk LC. In order to rationalize the shift of charge polarization phenomena towards lower temperatures with respect to pure E7, one has to assume that the colloidal mixtures exhibit a surprisingly higher conductivity than pure E7. Figure 16, which displays the temperature dependence of the conductivity as obtained from the dielectric spectra, indeed reveals a substantial increase of the conductivity for colloid-filled LC at all temperatures. As a consequence, the temperature at which the conductivity amounts to a certain value of say 10^{-9} S m^{-1} makes a down shift by almost 50°C between pure E7 and E7 with 6.4 wt % filler, which is in fair agreement with the temperature shifts noticed in figures 14(*a*) and 14(*b*).

Possible reasons for such a conductivity increase could be: (i) ionic impurities originating from the polymer filler phase, (ii) a change in the charge exchange/transfer rate at the electrodes, (iii) an intrinsic surface conductivity along the colloidal network, or (iv) a significant increase in the conductivity of bulk E7 due to elastic distortions of the director order and/or a high number of point defects.

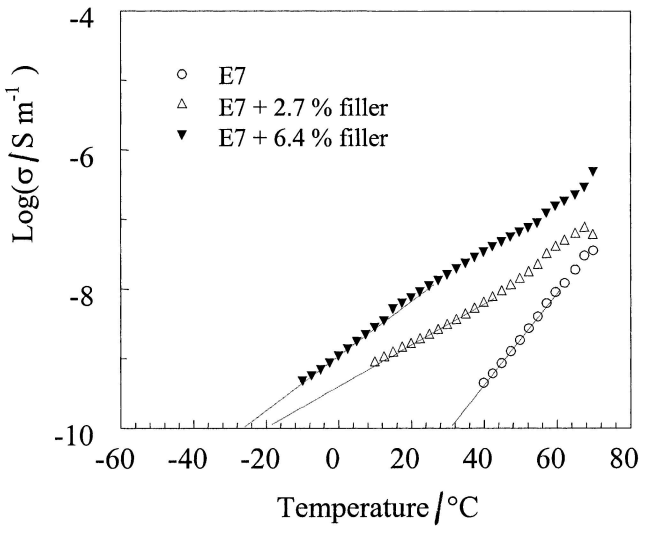

Figure 16. Temperature dependence of the conductivity of E7/colloid mixtures for three colloid contents: (○) 0 wt % (pure E7); (□) 2.7 wt %; (▼) 6.4 wt %.

4. Conclusions

Confocal laser scanning microscopy has shown that within colloidal dispersions in LCs the colloids are assembled in a three-dimensional network, by which the LC phase is confined within small cavities. Dielectric relaxation spectroscopy analysis on these two-phase materials indicates that the LC order in the non-addressed and addressed state, which was quantified by use of a director order parameter, becomes more distorted with increasing fraction of colloids. By use of a three-phase interlayer model the deviation from perfect alignment is expressed in terms of an interfacial shell between the filler particles and the aligned LC matrix, which comprises randomly oriented LC molecules. The thickness of the interfacial layer was found to decrease with (i) increasing d.c. bias and (ii) decreasing fraction of colloids.

Switching experiments at -40°C revealed a lowering of the threshold field when colloids were added to the LC. This is associated with a switching between two metastable states that are introduced by anchoring interactions between the LC and the filler particles. Electric field-induced changes in the dielectric spectra taken at -40°C reveal significant shifts of the α- and λ-relaxation peaks as well as the disappearance of the isosbestic points for higher colloid filler amounts. Detailed modelling of these spectra points to the existence of LC molecules with different mobilities within the colloidal dispersions.

With increasing colloid fraction a marked increase in ohmic conductivity was found over a broad range of temperatures. This causes a slow disorientation of the LC molecules after removal of a bias field, especially at lower temperatures around -10°C, and also gives rise to an 'abnormal' hysteresis in switching experiments. Below -30°C in all cases, also for the pure LC, the molecular dynamics are significantly slowed down, resulting in long decay times and 'normal' hysteresis effects in the switching curves.

This work was supported by The Netherlands Organisation for Applied Sciences (Stichting Toegepaste Wetenschappen, NWO-STW).

References

[1] Crawford, G. P., and Zumer, S., 1996, *Liquid Crystals in Complex Geometries: Formed by Polymer and Porous Networks*, edited by G. P. Crawford and S. Zumer (London: Taylor and Francis).

[2] Bellini, T., *et al*., 1992, *Phys. Rev. Lett*., **69,** 788.
[3] Dadmun, M. D., and Muthukumar, M., 1993, *J. chem. Phys*., **98,** 4850.
[4] Werner, J., *et al*., 2000, *Liq. Cryst*., **27,** 1295.
[5] Arndt, M., Stannarius, R., Gorbatschow, W., and Kremer, F., 1996, *Phys. Rev. E*., **54,** 5377.
[6] Jadzyn, J., Czechowski, G., Mucha, M., and Nastal, E., 1999, *Liq. Cryst*., **26,** 453.
[7] Golemme, A., Zumer, S., Allender, D. W., and Doane, J. W., 1988, *Phys. Rev. Lett*., **61,** 2937.
[8] Hikmet, R. A. M., and Zwerver, B. H., 1991, *Liq. Cryst*., **10,** 835.
[9] Haga, H., and Garland, C. W., 1997, *Phys. Rev. E*, **56,** 3044.
[10] Abd-El-Messieh, S. L., Werner, J., Schmalfuss, H., Weissflog, W., and Kresse, H., 1999, *Liq. Cryst*., **26,** 535.
[11] Alieve, F. M., Sinha, G. P., and Kreuzer, M., 2001, *Mol. Cryst. liq. Cryst*., **359,** 537.
[12] Cramer, C., Cramer, T., Kremer, F., and Stannarius, R., 1997, *J. chem. Phys*., **106,** 3730.
[13] Sinha, G. P., and Aliev, F. M., 1998, *Phys. Rev. E*, **58,** 2001.
[14] Ruhwandl, R. W., and Terentjev, E. M., 1997, *Adv. Mater*., **55,** 2958.
[15] Kuksenok, O. V., Ruhwandl, R. W., Shiyanovskii, S. V., and Terentjev, E. M., 1996, *Phys. Rev. E*, **54,** 5198.
[16] Poulin, P., Stark, H., Lubensky, T. C., and Weitz, D. A., 1997, *Science*, **275,** 1770.
[17] Loudet, J. C., Barois, P., and Poulin, P., 2000, *Nature*, **407,** 611.
[18] Poulin, P., Raghunathan, V. A., Richetti, P., and Roux, D., 1994, *J. Phys. II*, **4,** 1557.
[19] Van Boxtel, M. C. W., Janssen, R. H. C., Bastiaansen, C. W. M., and Broer, D. J., 2001, *J. appl. Phys*., **89,** 838.
[20] Petrov, P. G., and Terentjev, E. M., 2001, *Langmuir*, **17,** 2942.
[21] Meeker, S. P., Poon, W. C. K., Crain, J., and Terentjev, E. M., 2000, *Phys. Rev. E*, **61,** R6083.
[22] Anderson, V. J., Terentjev, E. M., Meeker, S. P., Crain, J., and Poon, W. C. K., 2001, *Eur. Phys. J. E*, **4,** 11.
[23] Anderson, V. J., and Terentjev, E. M., 2001, *Eur. Phys. J. E*, **4,** 21.
[24] Van Boxtel, M. C. W., Janssen, R. H. C., Broer, D. J., Wilderbeek, H. T. A., and Bastiaansen, C. W. M., 2000, *Adv. Mater*., **12,** 753.
[25] Kim, B. K., Kim, S. H., and Choi, C. H., 1995, *Mol. Cryst. liq. Cryst. Sci. Technol. A*, **261,** 605.
[26] Zhong, Z. Z., Schuele, D. E., Gordon, W. L., Adamic, K. J., and Akins, R. B., 1992, *J. polym. Sci*., **30,** 1443.
[27] Kresse, H., 1998, *Handbook of Liquid Crystals*, Vol. 2A, edited by D. Demus, J. W. Goodby, G. W. Gray, H.-W, Spiess and V. Vill (Chichester: Wiley-VCH), pp. 91–112; Dunmur, D., and Toriyama, K., 1998, *Handbook of Liquid Crystals*, Vol. 1, edited by D. Demus, J. W. Goodby, G. W. Gray, H.-W. Spiess and V. Vill (Chichester: Wiley-VCH), pp. 231–252.
[28] Attard, G. S., Araki, K., and Williams, G., 1987, *Br. polym. J*., **19,** 119.
[29] Steeman, P. A. M., 1992, PhD thesis, Delft University of Technology, Delft, The Netherlands.
[30] Priou, A., 1992, *Dielectric Properties of Heterogeneous Materials*, edited by A. Priou (Amsterdam: Elsevier).
[31] Feldman, Y., Skodvin, T., and Sjöblom, J., 2000, *Encyclopedic handbook of emulsion technology*, edited by J. Sjöblom (New York: Dekker), xxx.
[32] Steeman, P. A. M., and van Turnhout, J., 2002, *Dielectric Broadband Spectroscopy*, edited by F. Kremer and A. Schönhals (Berlin: Springer), xxx.
[33] Havriliak, S., and Negami, S., 1967, *Polymer*, **8,** 161.
[34] Looyenga, H., 1965, *Physica*, **31,** 401.
[35] Steeman, P. A. M., and Maurer, F. H. J., 1990, *Colloid polym. Sci*., **268,** 315.
[36] Mizoshita, N., Hanabusa, K., and Kato, T., 2001, *Displays*, **22,** 33.
[37] Jadzyn, J., Czechowski, G., Douali, R., and Legrand, C., 1999, *Liq. Cryst*., **26,** 1591.
[38] Batalla, B., Sinha, G., and Aliev, F., 1999, *Mol. Cryst. liq. Cryst. Sci. Technol. A*, **331,** 1981.
[39] De Jeu, W. H., 1980, *Physical Properties of Liquid Crystalline Materials* (London: Gordon and Breach).
[40] Wübbenhorst, M., and van Turnhout, J., *J. Non-Cryst. Solids* (in the press).
[41] Rout, D. K., and Jain, S. C., 1992, *Jpn. J. Appl. Phys., 1*, **31,** 1396.
[42] Hikmet, R. A. M., and Zwerver, B. H., 1992, *Liq. Cryst*., **12,** 319.